Dinitramide Ion: Robust Molecular Charge Topology Accompanies an Enhanced Dipole Moment in Its Ammonium Salt

James P. Ritchie,† Elizabeth A. Zhurova, Anthony Martin, and A. Alan Pinkerton*

Department of Chemistry, University of Toledo, 2801 West Bancroft Street, Toledo, Ohio 43606

Received: July 25, 2003; In Final Form: October 6, 2003

The electron density, $\rho(\mathbf{r})$, of crystalline ammonium dinitramide (ADN) was determined from low-temperature X-ray diffraction data and electronic structure calculations. Single molecule wave functions were also computed for comparison. Bader's atoms in molecules (AIM) method was used to partition $\rho(\mathbf{r})$. The same number and kinds of critical points in $\rho(\mathbf{r})$ for the dinitramide ion are found in ADN as were found in previous studies of other salts with different amounts of nitro group twist. An atomic interaction line (AIL) is always observed between the two "inner" oxygens. Topological characterization of the negative Laplacian of the charge distribution ($-\nabla^2\rho(\mathbf{r})$) was also performed to locate (3,−3) critical points in the valence-shell charge concentration (VSCC) region. Such points may be associated with the presence and location of lone pairs of electrons as predicted by the Lewis and VSEPR models. As with $\rho(\mathbf{r})$, the same number of (3,−3) critical points are found in the Laplacian, $-\nabla^2\rho(\mathbf{r})$, with experimental, single-molecule B3LYP, and crystal B3LYP models, however, comparison of experimental and theoretical results show some differences in the location of these points. These differences are shown to arise mostly from limited flexibility in the multipole model used to fit $\rho(\mathbf{r})$ to the experimental data. Nonetheless, both B3LYP modeling and experiment agree that there is a single (3,−3) critical point in the VSCC associated with a lone pair of electrons on the central nitrogen. The hybridization of the central nitrogen of the dinitramide ion is, therefore, sp^2-like, as observed in the two biguanidinium salts, $[((NH_2)_2C)_2N][N_3O_4]$ and $[((NH_2)_2C)_2NH][N_3O_4]_2$. Despite this robust topology, the dipole moment obtained from both experiment and crystal modeling is larger than that computed for a single dinitramide ion. Significant differences in the direction of the dipole from theory and experiment are found, as are differences in the atomic charges. These are also attributed to the limited flexibility of the multipole model. Electron densities obtained from crystal wave functions demonstrate that strong hydrogen bonding polarizes the dinitramide ion, increasing the negative charge on the most strongly hydrogen bonded oxygen atom. Decomposition of the theoretical molecular dipole moment into atomic charge and atomic dipole contributions reveals that the atomic dipoles are nearly equal in both the crystal and single molecular ion. Changes in the atomic charge contribution to the molecular dipole moment principally account for the induced dipole.

Introduction

The availability of a large number of dinitramide salts has presented the opportunity to examine the structure and electron density distribution of the dinitramide ion in a wide variety of environments. Nitro groups in the dinitramide ion, **I**, exhibit a

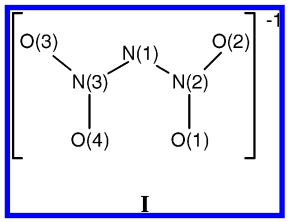

I

wide range of twist angles in crystal structures.[1] Electronic structure calculations at the B3LYP/6-311+G(d) level for the single molecular ion show that the potential energy surface has a minimum at a twist angle of 26° and C_2 symmetry.[2] The planar C_{2v} geometry lies but 1.8 kcal/mol higher in energy; it is a transition state for conversion between two enantiomeric C_2 minimum energy structures. A C_s conformation with one of the nitro groups twisted while the other is coplanar with the NNN plane lies 2.7 kcal/mol above the minimum energy structure. Further computations at this level with different amounts of nitro group twist show variations in geometric structure and atomic charges that are consistent with the operation of resonance delocalization.[1a] Finally, a survey of observed crystal structures shows that many of the nitro group twist angles lie within a flat region on the potential energy surface, and close to the line maintaining C_2 symmetry between the theoretical minimum and the planar structure.[1a] This survey also found structural and computational manifestations of strong steric repulsion between the "inner" oxygen atoms, O(1), O(4).

The variability in the structure of the dinitramide ion has led to a number of questions regarding its electronic structure. Despite the repulsion between "inner" oxygens evidenced in the crystal structures,[1a] experimental and theoretical analyses of the charge distribution using Bader's theory of atoms in molecules[3] (AIM) show atomic interaction lines (AIL's) exist between these atoms.[2,4] The presence of such AIL's between atoms with closed-shell interactions is an important factor in

* Corresponding author. E-mail: apinker@uoft02.utoledo.edu.
† Present address: Center for Computational Research; University at Buffalo; Buffalo, NY 14260-1800.

10.1021/jp036180r CCC: $25.00
Published on Web 11/25/2003

interpreting chemical bonding in molecules and crystals.[5] Other questions about the dinitramide ion stem from the suggestion that in the theoretical nonplanar minimum energy geometry, there are two electron lone pairs on a central sp^3 hybridized nitrogen which provide optimum conjugation with the nitro groups.[6] Furthermore, the survey of observed crystal structures shows that the NNN angles are always less than 120° and commonly in the range 112−117°.[1a] Although VSEPR theory predicts a closing of bond angles from formal values in the presence of lone pairs,[7] the size of the deviation of the NNN angle from 120° might be interpreted as evidence for an sp^3 hybridized central nitrogen.[6] Additional interest in the dinitramide anion stems from recent work questioning the location of lone pairs of electrons on oxygen in N_2O_4 at angles nearly orthogonal to the N−O bond; significant differences between theoretical and experimental atomic charges were also observed.[8] Finally, strong intermolecular interactions, including hydrogen-bonding, present in many dinitramide salts significantly affect the ion's geometry.[1a] This could significantly affect the electronic structure and charge density topology of the negative ion.

Bader's theory of atoms in molecules was used in previous work to analyze the experimentally based charge distributions of biguanidinium dinitramide (BIGH) and biguanidinium bis-dinitramide (BIGH2).[4] A single peak in the electron density deformation maps and the Laplacian associated with a lone pair of electrons was found on the central nitrogen of the dinitramide anion in both of these structures. AIL's were also found linking the "inner" oxygens in both cases. Significant conjugation is also evidenced by the observed ellipticity of the N−N bonds in these structures. Theoretical calculations discussed above show that the amount of conjugation will vary with the amount of nitro group twist.[1a] Consequently, ammonium dinitramide (ADN) was selected for further study. In the BIGH salt, the O−N−N−N dihedral angles with the inner oxygen atoms are 2.8 and 4.2°; in BIGH2, these angles are 23.1 and 9.5°; and in ADN, they are 27.9 and 22.8°. These three salts are thus representative of both nitro groups being nearly coplanar with the NNN plane (BIGH), only one of the groups being nearly so (BIGH2), and neither of the groups being nearly coplanar (ADN). The results provide insight into the properties of ADN using AIM theory, electronic structure calculations, and experimental methodology in characterizing the electron density, $\rho(\mathbf{r})$. We have also computed the "in crystal" dipole moment of the dinitramide ion using the AIM theory to partition the electronic charge. "In-crystal" dipole moment enhancements have been found in a wide variety of crystals[9] with enhancements in the range of 10−25% being well documented.[10] Many of these studies were, however, carried out with molecules containing a carbonyl group[11] or where conjugation is possible between an amine and a nitro group.[12,13] The dinitramide ion, in contrast, has none of these features and, furthermore, carries a total negative charge. Previous work with another salt, pyridinium dicyanomethylide, showed significant differences in the derived dipole moment depending upon the charge partitioning scheme.[14] AIM allows us to determine, in a manner free of arbitrary assumptions, the influence of intermolecular interactions upon the dipole and how its variation can be related to changes in the charge density topology of the ion.

Methods

A. Theory. The theory of atoms in molecules provides a means of partitioning a molecule into "atomic" regions and characterizing the interactions between them. It concerns the properties of regions in real space bounded by surfaces through which the flux in $\nabla\rho(\mathbf{r})$ is zero and is described in detail elsewhere.[3]

To obtain $\rho(\mathbf{r})$ from experimental or theoretical X-ray structure factors, the Hansen-Coppens (HC) multipole procedure was used.[15] In this method, the total electron density is represented as a sum of nonspherical atomic densities:

$$\rho(\mathbf{r}) = \sum \rho(\mathbf{r})_{\text{atom}} \tag{1}$$

These atomic densities may, in turn, be described with standard spherical core and valence distributions supplemented with a set of spherical harmonics (Y_{lm}) to describe valence shell deformations:

$$\rho(\mathbf{r})_{\text{atom}} = P_c\rho_{\text{core}} + P_v\kappa^3\rho_{\text{valence}}(\kappa\mathbf{r}) + \Sigma_l\kappa'^3 R_l(\kappa'\mathbf{r})\Sigma_m P_{lm} Y_{lm}(\theta,\phi) \tag{2}$$

Values of κ, κ', P_v, and P_{lm} may be found for each atom through least-squares minimization with respect to observed and calculated structure factors. The choice of the additional parameters of the model, including the number, kind, and location of the spherical harmonics and radial functions used in eq 2, is governed by practical considerations and are known to pose significant limits on the flexibility and accuracy of the density distribution thus obtained.[16] In this work, an electron density determined using eqs 1 and 2 will be referred to as a "multipole fit". It can be used directly to obtain topological quantities of the charge density distribution in the crystal.

A charge distribution may also be computed using a wave function from an electronic structure calculation, as shown in eq 3. In this equation, $P_{\mu v}$ is the density matrix element

$$\rho(\mathbf{r}) = \sum_{\mu v} P_{\mu v}\varphi_\mu(\mathbf{r})\,\varphi_v(\mathbf{r}) \tag{3}$$

multiplying the AO's φ_μ and φ_v. Herein, we shall refer to the charge distribution obtained from eq 3 as a "theoretical charge distribution". It can also be used directly for AIM analysis, or to obtain "theoretical structure factors". As these pertain to an actual, even if approximate, electron density distribution, they are free of contributions from effects mentioned above that are found in "real" crystals.[17] Consequently, theoretical structure factors can be viewed as "error free" data for a precisely given model electron density.

Theoretical structure factors can also be used to obtain the multipole expansion parameters via least-squares minimization. This procedure is analogous with that performed using observed structure factors; however, the electron density distribution is already known from eq 3. This electron density can then be used in the topological analysis to check the results from the multipole expansions. Ideally, topological analysis of the theoretical density and that obtained by multipole fit to the theoretical structure factors should be identical. But, as has been previously observed, significant differences are found.[16]

Herein we report topological analyses for the dinitramide anion with three different types of charge distributions: one obtained from experimentally observed structure factors via least squares minimization, one obtained from theoretical structure factors in the same fashion, and one obtained directly from the molecular or crystal wave function. Use of these different densities allows us to determine effects due to the multipole fitting procedure that is a necessary part of the experimental work. We also report theoretical charge distributions for both the crystal and a single dinitramide ion to determine changes induced by the crystal environment.

TABLE 1: Summary of Computational Models and Acronyms Used in This Work

acronym	description
X	multipole fit of experimentally observed X-ray structure factors using XD programs
SCF	single molecule self-consistent field molecular orbital calculation using GAUSSIAN98;[a] topological parameters obtained from AIMPAC[b]
PSCF	periodic self-consistent field calculations performed with CRYSTAL98;[c] TOPOND[d] analysis of $\rho(\mathbf{r})$ using wave function from CRYSTAL98
MPSCF	multipole fit using XD programs[e] with structure factors calculated from above model; TOPXD[f] analysis of $\rho(\mathbf{r})$ using all F_{hkl}'s inside a 1.05 Å^{-1} Ewald sphere
DFT	single molecule calculation using GAUSSIAN98[a] with "B3LYP" keyword; topological parameters obtained from AIMPAC[b]
PDFT	periodic calculations performed with CRYSTAL98[c] using "B3LYP" functional; TOPOND[d] analysis of $\rho(\mathbf{r})$ obtained from CRYSTAL98
MPDFT	multipole fit using XD programs[e] with structure factors calculated from above model; TOPXD[f] analysis of $\rho(\mathbf{r})$ using all F_{hkl}'s inside of 1.05 Å^{-1} Ewald sphere

[a] Reference 19. [b] Reference 21. [c] Reference 22. [d] Reference 23. [e] Reference 24. [f] Reference 9b.

B. Modeling. Table 1 briefly describes the computational models and representative acronyms used in this work. All computations were performed on one of three commercial desktop PC's. The 6-21G** basis set[18] and a molecular geometry fixed at that observed experimentally were used throughout (see Experimental Section).

Single molecule wave functions were obtained with GAUSSIAN98[19] using both the SCF and B3LYP methods.[20] Topological characterization of the corresponding electron density distribution obtained from eq 3 was performed with AIMPAC.[21] Results from the single molecule calculations are denoted by "SCF" and "DFT". Periodic wave functions were computed using these same basis functions and Hamiltonians in the CRYSTAL98 program.[22] Topological analysis of the corresponding periodic charge distribution from eq 3 was performed using the TOPOND98 program.[23] Results from these models are denoted by "PSCF" and "PDFT". To determine the effect of the multipole-fitting procedure, CRYSTAL98 was used to obtain theoretical structure factors within the range of $0.0 \le \sin\theta/\lambda \le 1.05$ Å^{-1} (see below). These were used, in turn, in the XD program suite[24] to determine a multipole-fit electron density, described in eqs 1 and 2. Results from this procedure are denoted MPSCF and MPDFT. The program TOPXD[9b] was then used to characterize the desired topological parameters. Finally, structure factors from the X-ray experiment were used with the XD programs to obtain a multipole-fit electron density. Topological characterization of the resulting density was performed using TOPXD. Results from this procedure are denoted by "X".

C. Experimental and Refinements. Crystals of ammonium dinitramide were grown by slow evaporation from dry acetonitrile solution. A colorless crystal plate with well-defined faces was then selected for the diffraction experiments and mounted on a fine glass capillary. Preliminary examination and data collection were performed with Mo Kα radiation using an Enraf-Nonius CAD4 κ axis diffractometer equipped with an Oxford Cryostream cooling device. Cell constants and an orientation matrix were obtained from the setting angles of 25 reflections measured by the diagonal slit method of centering, followed by least-squares refinement (Table 2). The intensity data were collected using the $\omega-2\theta$ scan technique using a variable scan rate (0.9−5.5°/min). A full sphere of data up to $\sin\theta/\lambda = 1.34$ Å^{-1} was collected (Table 2). For the high-angle data, only those reflections calculated[25] to be greater than $3\sigma(I)$ were measured. The stability of the experiment was checked by measuring 3 representative orthogonal reflections every 60 min. Data reduction[26] was carried out in the following manner. The peak profiles were analyzed, and Lorentz and polarization corrections applied to the data using the programs REFPK and BGLP. A linear scaling correction was applied using the computer program SCALE3. An analytical absorption correction was applied using the program ABSORB,[27] followed by a correction for errors in the measured crystal shape, absorption due to the capillary and glue, and X-ray beam inhomogeneity using the program SORTAV. An empirical TDS correction was applied using the computer program TDSCORR, the maximum intensity correction applied being 24.9%.

TABLE 2: Crystal Data and Structure Refinements

empirical formula	$NH_4{\cdot}N_3O_4$ ($N_4H_4O_4$)
temperature	90(1) K
crystal size	0.27 × 0.21 × 0.09 mm
space group	$P2_1/c$
unit cell dimensions	$a = 6.933(1)$, $b = 11.603(1)$, $c = 5.567(1)$ Å, $\beta = 100.58(1)°$
Unit cell θ range	$8 < \theta < 16°$
V, Z	440.2 Å^3, 4
$\omega/2\theta$ scan width	$0.8 + 0.34 \tan\theta$, deg
absorption coefficient	0.1798 mm^{-1}
2θ range	5.98−146.0, $(\sin\theta/\lambda)_{max} = 1.34$ Å^{-1}
no. of reflections collected	21641
no. of independent reflections	5547, ($R_{int} = 0.0224$)
no. of reflections used ($I > 4\sigma(I)$)	3602
refinement method	full-matrix least-squares on F
weighting scheme	$1/\sigma^2(F_{obs})$
no. of parameters	264
final R indices:	
spherical atom refinement	0.0292
aspherical atom refinement	0.0197
goodness-of-fit (aspherical)	0.79

The crystal structure was resolved and preliminary refinements using the traditional spherical atom model were carried out with the SHELXTL program suite.[28] For subsequent refinements, the Hansen-Coppens multipole model[15] as implemented in the XD program[24] was employed using the following strategy. The positional and displacement parameters for the non-hydrogen atoms were refined using the high-angle reflections ($\sin\theta/\lambda > 0.7$ Å^{-1}). For hydrogen atoms, the positional and displacement parameters were refined using data with $\sin\theta/\lambda < 0.5$ Å^{-1}, then, the N−H bond lengths were extended and fixed to the tabulated neutron values.[29] The multipole P_v, P_{lm}, κ, κ' parameters and extinction were refined with the low-angle reflections ($\sin\theta/\lambda < 1.0$ Å^{-1}). The scale factor refinement was carried out with all reflections, the procedure being repeated until convergence. For the heavy atoms (C, N, O), the multipole refinement was only performed up to the octupole level ($l_{max} = 3$) as all of the hexadecapole ($l_{max} = 4$) parameters were found to refine to statistically insignificant values. For the hydrogen atoms, only dipole and quadrupole ($l_{max} = 2$) populations were refined. The electroneutrality condition was imposed during all refinements. A total of five κ sets were used in the refinements with one value for all the oxygen atoms, one for all the hydrogens, but three values for the chemically distinct nitrogen atoms. Isotropic secondary extinction type I with a Gaussian mosaic distribution was described following Becker and Coppens,[30] the y_{min} values being 0.76, 0.87, and 0.95 for the (040), ($\bar{1}2\bar{1}$), and ($23\bar{1}$) reflections, respectively. The rigid-bond test[31]

TABLE 3: Optimized Parameters from the Hansen−Coppens Multipole Fitting Procedure[a]

	PSCF	PDFT	X
$R(F)$ (%)	0.59	0.63	1.57
κ/κ'			
O	0.9718/1.0892	0.9814/1.1106	0.9860/1.0448
N(1)	0.9809/0.9740	0.9907/0.9946	0.9917/0.9977
N(2),N(3)	0.9693/0.7946	0.9948/0.7869	1.0003/0.8497
N(4)	0.9828/0.8596	0.9923/0.8365	0.9696/0.8126
H	1.1591/1.3236	1.1679/1.3696	1.1216/1.1062

[a] All 4268 unique nonzero reflections within a 1.05 Å^{-1} Ewald sphere were considered with the theoretical structure factors. Experimental structure factors are described in the Methods section. Lists of all optimized parameters are available in the Supporting Information. For abbreviations, see Table 1.

showed that no difference of mean-square displacements along interatomic vectors were greater than 2×10^{-4} Å^2. No least-squares correlation coefficient was greater than 0.30. A list of the final refined parameters accompanies this manuscript as Supporting Information.

Results and Discussion

A. Refinements. Table 3 summarizes quantities obtained from refinements using both theoretical and experimental structure factors. The different ranges of sin θ/λ for selection of structure factors in the multipole refinements (sin $\theta/\lambda < 1.0$ Å^{-1} for the observed and sin $\theta/\lambda < 1.05$ Å^{-1} for those from theory) are expected to have no significant effect on the conclusions of this study. The multipole expansions of the electron density used complete sets of spherical harmonics including up to octupoles on heavy atoms and up to quadrupoles on hydrogen. The low R_F values obtained for the theoretical charge distributions indicate that the minimization criterion is largely satisfied. A larger value is obtained for refinement of the experimental data, but the R_F is still low for such refinements. Values of κ and κ', shown in Table 3, were also refined along with the multipole populations. The values obtained for κ are consistent with net negative charges on oxygen, whereas those on the nitrogens differ somewhat from a simple correlation.[32] Even though κ' values differ from model to model, values for N(1) are consistently larger than those found for N(2) and N(3), which have more substituents. It is particularly noticeable that κ' values for hydrogen are significantly larger in the refinements using theoretical structure factors than when using experimental ones. This suggests that a more diffuse charge distribution around hydrogen is obtained from experimental data.

B. Topology of the Electron Density, $\rho(\mathbf{r})$. Table 4 lists results from the topological characterization of $\rho(\mathbf{r})$ from different sources. All methods give the same number and kind of critical points for the dinitramide anion. In addition to those expected for strong covalent bonds, an AIL is always found between the inner oxygen (O(1) and O(4)) atoms, as well as a ring (O(1), O(4), N(1), N(2), N(3)) critical point, thus satisfying the Hopf-Poincaré relation.[3] At the critical points between the oxygen atoms and in the ring, the observed values of the electron density, ρ_c, are low, close to the estimated uncertainty in $\rho(\mathbf{r})$ of the experiment; however, they are reproduced by the calculations. Values of the Laplacian at the O(1)···O(4) critical point, $\nabla^2\rho_c$, obtained from the MPSCF and MPDFT differ by less than 10%, compared with experiment. Also, comparing SCF/PSCF and DFT/PDFT results shows that these critical points are only slightly affected by the crystal environment. But, PSCF/MPSCF and PDFT/MPDFT comparisons show that values of ρ_c and $\nabla^2\rho_c$ are reduced by the multipole fit from the theoretical structure factors. The ellipticity for the O···O AIL is highly variable; however, as it is a ratio of small quantities, it is subject to large errors.

Further inspection of other values of ρ_c and $\nabla^2\rho_c$, in Table 4 and Figures 1 and 2, reveals some additional systematic trends. Qualitatively, the values are typical for strong covalent bonds. Computed values of ρ_c from MPDFT are frequently smaller than those obtained from experiment, sometimes by as much as 10%. Also, a trend showing a decrease in all values of ρ_c from the multipole fits is evident in PSCF/MPSCF and PDFT/MPDFT comparisons. Only very small changes in ρ_c can be attributed to the crystal environment as SCF/PSCF and DFT/PDFT comparisons typically show differences in this quantity of less than 1%. Corresponding changes in $\nabla^2\rho_c$ due to the crystal environment also range over a few percent and the limited range is even more striking than for ρ_c.

Figure 1 shows a plot of the electron density at the bond critical points in the dinitramide anion, ρ_c, organized in the order of the corresponding bond lengths. For the N−O bonds, all levels of theory uniformly rank ρ_c in the reverse order of bond length, consistent with bond-order/bond-length/ρ_c relations.[32] The experimental results are not quite as uniform; however, the differences among the first three members of this series are not large, the experimental values of ρ_c being identical within the statistical error (∼0.02 e/Å^{-3}). The computed results for these three bonds show approximately 4% variation in ρ_c (at MPDFT: ρ_c[N(2)−O(1)]/ρ_c[N(3)−O(3)] = 1.039). This is also in agreement with values of ρ_c from previous experiments with the BIGH and BIGH2 salts: two of the N−O bonds in these salts have identical lengths of 1.248 Å and the ratio of ρ_c for these bonds is 1.038.

Figure 2 shows a similar comparison of the values of the Laplacian at the bond critical points, $\nabla^2\rho_c$, for the various bonds in the dinitramide anion. Again, the MPSCF and MPDFT values are usually close to those obtained from the observed structure factors. However, a significant difference for the N(2)−O(2) bond suggests a possible error in the experimental value. We may also compare quantities associated with the two N−N bonds in different salts of dinitramide. The ratio of these bond lengths in ADN is R[N(1)−N(3)]/R[N(1)−N(2)] = 1.011. Ratios of ρ_c from the different theoretical calculations are essentially identical $-\rho_c$[N(1)−N(2)]/ρ_c[N(1)−N(3)] = 1.030−1.035. A larger value of 1.111 is found from the experiment. These ratios again suggest that there may be some error in the experimental electron density. Deformation electron density maps (deposited) show significantly greater buildup of electron density in the shorter bond compared with the longer one. Comparing similar ratios from the BIGH and BIGH2 salts, for BIGH2, R[N(1)−N(2)]/R[N(1)−N(3)] = 1.027 and ρ_c[N(1)−N(3)]/ρ_c[N(1)−N(2)] = 1.13; for BIGH, R[N(1)−N(3)]/R[N(1)−N(2)] = 1.016 and ρ_c[N(1)−N(2)]/ρ_c[N(1)−N(3)] = 1.056, reveals that the bond length ratio is somewhat larger than that in ADN; however, only for a bond length ratio of 1.027 does the ρ_c ratio reach that observed for ADN.

One trend particularly noticeable in Table 4 is the known[16] error in values of $\nabla^2\rho_c$ caused by lack of flexibility in the multipole fits. Much more positive values are found using the multipole method, than when using the theoretical charge distribution. Further, it is observed that the error in values of $\nabla^2\rho_c$ results principally from λ_3, the curvature along the direction of the bond path. Values of the ellipticity, ϵ [$\epsilon = \lambda_1/\lambda_2 - 1$], obtained from PSCF/MPSCF and PDFT/MPDFT also reflect this effect.

TABLE 4: Quantities Associated with Non-Nuclear Critical Points in the Electron Density of the Dinitramide Anion Computed from the Different Models[a]

	linked atoms	type	ρ_c	$\nabla^2\rho_c$	d_i, d_j (Å)	λ_1	λ_2	λ_3	ϵ
X	(none)	(3,+1)	0.109	2.66	1.324 [O(1)] 1.350 [O(4)] 1.549 [N(1)]	−0.23	0.51	2.38	
SCF			0.137	3.11	1.341 [O(1)] 1.341 [O(4)] 1.532 [N(1)]	−0.40	0.50	3.01	
PSCF			0.137	3.04	1.333 [O(1)] 1.331 [O(4)] 1.568 [N(1)]	−0.41	0.37	3.08	
MPSCF			0.115	2.91	1.331 [O(1)] 1.330 [O(4)] 1.574 [N(1)]	−0.28	0.49	2.70	
DFT			0.142	2.92	1.336 [O(1)] 1.335 [O(4)] 1.552 [N(1)]	−0.43	0.37	2.98	
PDFT			0.140	2.83	1.326 [O(1)] 1.323 [O(4)] 1.602 [N(1)]	−0.45	0.22	3.06	
MPDFT			0.115	2.74	1.322 [O(1)] 1.321 [O(4)] 1.614 [N(1)]	−0.29	0.32	2.72	
X	O(1)−O(4)	(3,−1)	0.116	2.25	1.291, 1.300	−0.38	−0.32	2.95	0.18
SCF			0.143	2.71	1.295, 1.295	−0.54	−0.38	3.63	0.43
PSCF	$R = 2.586$		0.140	2.74	1.296, 1.296	−0.52	−0.30	3.56	0.74
MPSCF			0.120	2.42	1.294, 1.293	−0.40	−0.32	3.13	0.22
DFT			0.145	2.58	1.298, 1.297	−0.54	−0.30	3.43	0.81
PDFT			0.141	2.63	1.299, 1.301	−0.51	−0.19	3.34	1.68
MPDFT			0.117	2.40	1.300, 1.299	−0.37	−0.24	3.01	0.59
X	N(3)−O(4)	(3,−1)	3.426	−13.81	0.596, 0.632	−33.18	−28.27	47.64	0.17
SCF			3.426	−38.17	0.575, 0.652	−32.08	−28.24	22.16	0.14
PSCF	$R = 1.227$		3.413	−37.64	0.575, 0.652	−32.60	−28.83	23.80	0.13
MPSCF			3.268	−13.88	0.615, 0.612	−27.63	−25.46	39.21	0.09
DFT			3.335	−31.93	0.561, 0.667	−30.63	−27.39	26.10	0.12
PDFT			3.320	−31.43	0.561, 0.666	−31.03	−27.92	27.52	0.11
MPDFT			3.167	−8.78	0.600, 0.627	−26.95	−24.86	43.04	0.08
X	N(3)−O(3)	(3,−1)	3.440	−14.33	0.599, 0.637	−34.05	−28.40	48.12	0.20
SCF			3.367	−36.77	0.586, 0.650	−31.60	−27.65	22.48	0.14
PSCF	$R = 1.236$		3.354	−36.34	0.584, 0.652	−32.34	−28.13	24.13	0.15
MPSCF			3.200	−12.77	0.620, 0.616	−27.11	−24.65	38.99	0.10
DFT			3.277	−30.93	0.570, 0.666	−30.36	−26.85	26.28	0.13
PDFT			3.265	−30.44	0.568, 0.668	−31.06	−27.24	27.86	0.14
MPDFT			3.100	−7.76	0.604, 0.631	−26.52	−24.08	42.84	0.10
X	N(2)−O(1)	(3,−1)	3.420	−14.81	0.595, 0.626	−33.89	−27.78	46.86	0.22
SCF			3.469	−39.40	0.569, 0.652	−32.55	−28.72	21.88	0.13
PSCF	$R = 1.222$		3.463	−38.53	0.572, 0.650	−33.04	−29.01	23.52	0.14
MPSCF			3.320	−14.52	0.612, 0.609	−28.14	−25.91	39.54	0.09
DFT			3.377	−33.03	0.556, 0.666	−31.05	−27.84	25.86	0.12
PDFT			3.374	−32.50	0.559, 0.663	−31.47	−28.23	27.20	0.11
MPDFT			3.220	−9.36	0.599, 0.622	−27.40	−25.29	43.33	0.08
X	N(2)−O(2)	(3,−1)	2.944	−3.74	0.624, 0.630	−25.92	−21.94	44.12	0.18
SCF			3.219	−32.33	0.608, 0.647	−29.75	−26.08	23.49	0.14
PSCF	$R = 1.255$		3.208	−32.79	0.602, 0.653	−30.73	−26.90	24.84	0.14
MPSCF			3.052	−10.04	0.633, 0.623	−25.47	−22.97	38.39	0.11
DFT			3.131	−27.15	0.589, 0.667	−28.76	−25.42	27.03	0.13
PDFT			3.121	−27.30	0.584, 0.672	−29.75	−26.00	28.45	0.14
MPDFT			2.951	−5.19	0.615, 0.639	−24.96	−22.42	42.20	0.11
X	N(1)−N(3)	(3,−1)	2.281	−6.13	0.660, 0.714	−19.71	−16.14	29.72	0.22
SCF			2.480	−24.41	0.602, 0.771	−22.06	−16.77	14.42	0.32
PSCF	$R = 1.372$		2.452	−23.68	0.610, 0.763	−22.39	−17.12	15.83	0.31
MPSCF			2.282	−7.04	0.627, 0.746	−18.78	−14.44	26.18	0.30
DFT			2.431	−21.12	0.640, 0.732	−21.79	−17.66	18.33	0.23
PDFT			2.404	−20.31	0.644, 0.729	−21.94	−17.76	19.39	0.24
MPDFT			2.226	−3.59	0.651, 0.720	−18.08	−14.54	29.04	0.24
X	N(1)−N(2)	(3,−1)	2.532	−8.88	0.643, 0.715	−22.95	−17.69	31.76	0.30
SCF			2.558	−26.02	0.592, 0.766	−22.94	−16.98	13.90	0.35
PSCF	$R = 1.357$		2.525	−24.85	0.596, 0.762	−23.09	−17.05	15.29	0.35
MPSCF			2.361	−8.01	0.618, 0.740	−19.67	−14.85	26.52	0.32
DFT			2.509	−22.98	0.631, 0.727	−22.62	−18.08	17.72	0.25
PDFT			2.483	−22.04	0.632, 0.727	−22.73	−18.06	18.74	0.26
MPDFT			2.305	−4.57	0.643, 0.715	−18.94	−15.09	29.47	0.26

[a] Internuclear separations (R) are shown for atoms linked by an AIL. The type is shown as the rank and signature of the Hessian matrix. Also shown are the total electron density at the critical point (ρ_c), the Laplacian of the total density at the critical point ($\nabla^2\rho_c$), the distance from each critical point to the linked atoms (d_i, d_j), the eigenvalues of the Hessian (λ_1, λ_2, and λ_3), and the ellipticity (ϵ). Electrons and Ångstroms are used throughout. For abbreviations, see Table 1.

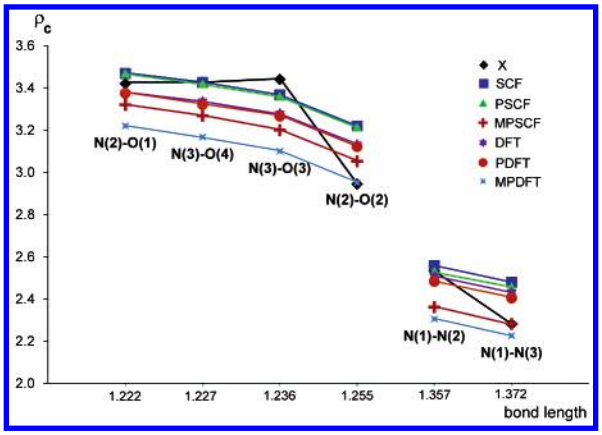

Figure 1. Electron density values (e Å^{-3}) at the bond critical point for the N−O and N−N bonds ordered according to type and bond length.

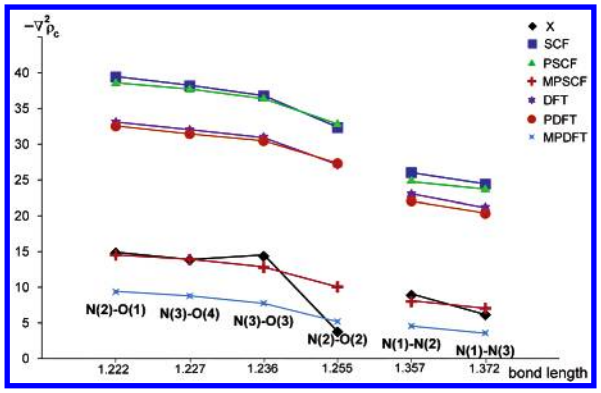

Figure 2. Negative Laplacian of the electron density (e Å^{-5}) at the bond critical point, $-\nabla^2\rho_c$, for the N−O and N−N bonds ordered according to type and bond length.

As with the BIGH and BIGH2 salts, the ellipticity of the N−N bonds is found to be high in ADN, indicative of significant π-character. Both the experimental and numerical results are in close agreement for these bonds. Ellipticities of the N−O bonds are in the range 0.17−0.22 from experiment, again indicating significant π-character in these bonds. The computational results for the ellipticities in the MPSCF and MPDFT models are lower than obtained from the PSCF/SCF and PDFT/DFT calculations, again indicating some distortions due to the multipole procedure. However, the ellipticities obtained from the PSCF/SCF and PDFT/DFT calculations are closer to those from the experiment.

C. Topology of Hydrogen Bonds. Although other weak hydrogen bonds may be identified (see below), four distinctly short hydrogen bonds are found in ADN. The R(O···H) internuclear distances for these four hydrogen bonds fall in the narrow range from 1.982 to 2.084 Å. An O(4)···H(3) separation of 2.406 Å is the next largest distance, thus these four hydrogen-bonds are well-separated from any others. Table 5 and Figures 3 and 4 show quantities derived from the topological analysis of these bonds. As expected, ρ_c decreases with increasing values of R(O···H) in both experiment and theory. Values of $\nabla^2\rho_c$ are uniformly positive, but show large percentage differences between theory and experiment, as do values of ϵ. Other hydrogen-bond critical points were found in the model densities, but values of ρ_c did not exceed 0.1 e/Å^3 and were ignored in this study. Values of ρ_c for the closest contacts from experiment are in the range found in the BIGH and BIGH2 salts.

It can also be observed that each of the four hydrogen atoms in the ammonium ion participates in just one of these four short hydrogen bonds. Moreover, as shown in Table 5, of the shortest hydrogen bonds in ADN, one each is to O(3) and O(4), whereas O(2) participates in two of these interactions. O(1) lacks such a strong hydrogen bond and there is no such close H···N(1) contact.

D. Atomic Charges. Table 6 shows atomic charges, dipole magnitudes, and values of the Lagrangian ($-^1/_4\nabla^2\rho$) obtained by integration of the charge distributions for dinitramide ion within the zero-flux surfaces. In addition, charges obtained from the Hansen−Coppens multipole fit, when available, are shown for comparison. Total charges and dipoles for the dinitramide ion are shown at the bottom of Table 6. Some differences may be noted between the experimental and computed values of this quantity. The experimental charge indicates only a small amount of anion to cation charge transfer, 0.03 e, whereas the MPDFT model gives 0.13 e, a significant amount. This value is smaller than that found experimentally in the BIGH salt (0.29), whereas a value of −0.09 is obtained for BIGH2. Thus, the computed values are in the range of those found by experiment on other systems.

The charge at N(1) is of particular interest. The MPDFT model reproduces the experimental result and differs by only 0.02 e from that obtained for a single molecular ion. This shows that N(1) is relatively unperturbed by the crystal environment. SCF/PSCF and DFT/MPDFT comparisons of the atomic dipole of N(1) also show only a very small effect wrought by either the crystal or the multipole fit.

In contrast with N(1), charges on oxygen show significant perturbations by the crystal lattice. Significant effects are also introduced by the multipole fitting procedure. As a reference point, the single molecule models show only very small variations among the charges on the different oxygen atoms; the entire range being 0.01 e. In the experiment, O(1) is found to have the least negative charge with the same value in both the X and MPDFT models. It also does not have a strong hydrogen bond. Other oxygens in the X model have the same charges, but the theoretical calculations show significant effects of the multipole fitting procedure. For example, in the PDFT model, O(2) bears the largest charge, whereas the remaining O(3) and O(4) atoms have equal charges, the total range being 0.09 e. In the MPDFT model this range is reduced to 0.04 e, but the ordering remains the same: O(1) is least negative, whereas O(2) is most negative. A similar trend is found in the SCF series.

Information about resonance interactions should be obtained by comparing the total charge on the nitro groups with that found in BIGH and BIGH2, as shown below in Table 7. Even though one of the nitro groups in BIGH is an outlier, the entire range of the remaining experimental results is similar to that introduced by hydrogen bonding: approximately 0.1 e. These nitro group charges are qualitatively reasonable but indicate the presence of effects other than resonance.

E. Topology of the Laplacian. The topology of $-\nabla^2\rho(\mathbf{r})$ in the valence shell charge concentrations (VSCC) shows regions of concentration and depletion in the electron density that may be associated with the electron lone pairs (lp) of the Lewis model.[3] Further, the location of such (3,−3) critical points is related to the hybridization of the atom. Table 8 displays a number of properties of pairs of (3,−3) critical points associated with the oxygen atoms of the dinitramide ion. Such points near N(1) merit special consideration and will be discussed separately below.

As with critical points in $\rho(\mathbf{r})$, there is agreement to approximately 5% between the experimental and theoretical

TABLE 5: Quantities at the Bond Critical Point in Some Hydrogen Bonds in Ammonium Dinitramide[a]

	linked atoms	type	ρ_c	$\nabla^2\rho_c$	d_i, d_j (Å)	λ_1	λ_2	λ_3	ϵ
X	O(3)···H(4)	(3,−1)	0.195	0.94	1.244, 0.747	−1.200	−1.080	3.22	0.12
PSCF			0.161	2.09	1.304, 0.680	−0.852	−0.831	3.77	0.02
MPSCF	$R = 1.982$		0.171	1.43	1.256, 0.727	−0.963	−0.916	3.31	0.05
PDFT			0.177	1.83	1.291, 0.692	−0.928	−0.913	3.67	0.02
MPDFT			0.180	1.49	1.236, 0.754	−0.996	−0.960	3.45	0.04
X	O(2)···H(1)	(3,−1)	0.142	1.20	1.286, 0.805	−0.899	−0.691	2.79	0.30
PSCF			0.149	1.97	1.324, 0.690	−0.768	−0.756	3.49	0.02
MPSCF	$R = 2.013$		0.160	1.35	1.269, 0.746	−0.881	−0.838	3.07	0.05
PDFT			0.165	1.74	1.310, 0.703	−0.834	−0.829	3.40	0.01
MPDFT			0.168	1.42	1.248, 0.768	−0.912	−0.873	3.20	0.05
X	O(2)···H(2)	(3,−1)	0.131	1.22	1.303, 0.766	−0.830	−0.547	2.60	0.52
PSCF			0.133	1.85	1.349, 0.720	−0.675	−0.661	3.19	0.02
MPSCF	$R = 2.068$		0.138	1.29	1.296, 0.773	−0.728	−0.682	2.70	0.07
PDFT			0.147	1.66	1.336, 0.733	−0.730	−0.726	3.11	0.01
MPDFT			0.146	1.35	1.275, 0.799	−0.759	−0.719	2.83	0.06
X	O(4)···H(3)	(3,−1)	0.113	1.05	1.321, 0.781	−0.635	−0.564	2.25	0.13
PSCF			0.113	1.69	1.346, 0.739	−0.561	−0.546	2.79	0.03
MPSCF	$R = 2.084$		0.124	1.12	1.310, 0.776	−0.644	−0.607	2.37	0.06
PDFT			0.125	1.55	1.333, 0.752	−0.616	−0.604	2.77	0.02
MPDFT			0.131	1.18	1.293, 0.799	−0.667	−0.636	2.49	0.05

[a] Internuclear separations (R) are shown for atoms linked by an AIL. The type is shown as the rank and signature of the Hessian matrix. Also shown are the total electron density at the critical point (ρ_c), the Laplacian of the total density at the critical point ($\nabla^2\rho_c$), the distance from each critical point to the linked atoms (d_i, d_j), the eigenvalues of the Hessian (λ_1, λ_2, and λ_3), and the ellipticity (ϵ). Electrons and Ångstroms are used throughout. For abbreviations, see Table 1.

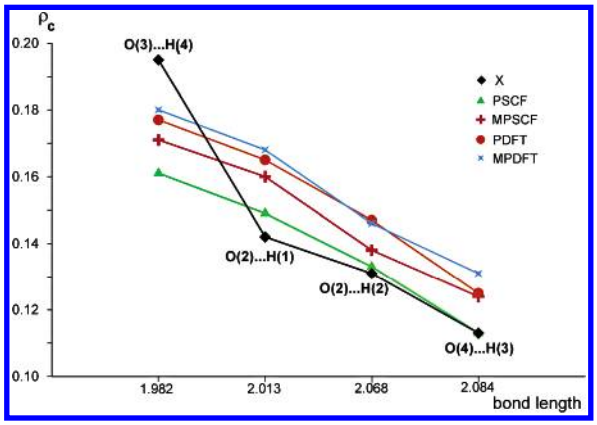

Figure 3. Electron density values (e Å^{-3}) for the strongest hydrogen bonds ordered according to type and bond length.

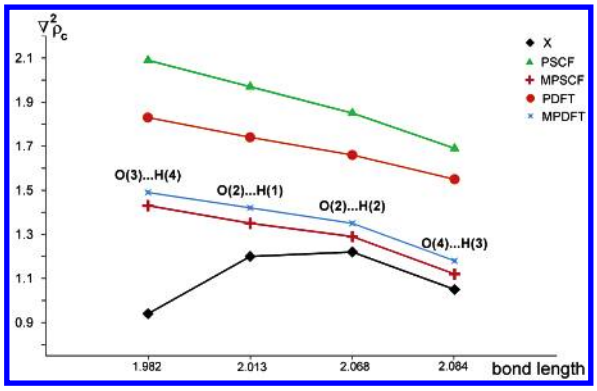

Figure 4. Laplacian values (e Å^{-5}) for the strongest hydrogen bonds ordered according to type and bond length.

values of $\rho(\mathbf{r})$ at the critical points of the Laplacian. However, significant differences are again found between theoretical and experimental values of $\nabla^2\rho_c$. Comparisons of PSCF/MPSCF and PDFT/MPDFT show this also to be the result of the multipole fitting protocol.

Comparisons of values of ρ_c and $\nabla^2\rho_c$ from SCF/PSCF and DFT/PDFT show only small effects for ρ_c, but larger ones for $\nabla^2\rho_c$. In particular, values of this quantity for O(2) exhibit the largest changes and may be attributed to the two strong hydrogen bonds to this atom. Examination of the crystal structure shows that these bonds are oriented nearly along the lp−O direction and are nearly coplanar with the nitro group. In accordance with these observations, $\nabla^2\rho_c$ undergoes the least change at O(1) in the SCF/PSCF and DFT/PDFT comparisons, whereas those at O(3) and O(4) undergo intermediate changes.

We note that all VSCC critical points lie within the range 0.333−0.340 Å from the nucleus and that these values are relatively unchanged by the multipole fitting procedure.

The positions of the lone pairs on oxygen are also of interest, as they are normally conceived to occupy hybrid molecular orbitals that are formally at angles with the NO internuclear axis of 120° for sp^2 hybridization and 109.5 for sp^3 hybridization. The experimental angles span the range 93.2−114.6°, whereas the MPDFT model spans a narrower range from 99.3 to 103.7°. The multipole fitting procedure produces changes in this angle by as much as 3°, which is comparable in size to the changes found associated with the incorporation of the ion into the lattice.

The dihedral angles formed by the (3,−3) critical points with the atoms of the nitro group are also of importance. The theoretical models consistently show that these critical points are nearly coplanar with each other and the O−N atoms, never being twisted more than a few degrees out of the nitro group plane. Experimentally, these critical points are found significantly further out of the plane of the nitro group in three out of four atoms, but at O(1), their experimental location corresponds quite closely with that obtained in the models. We note that this atom lacks the strong hydrogen bonding of the other oxygen atoms, suggesting a possible origin for this effect.

The angle formed by the lone pairs with the N−O bond lie close to 100°. This value is small for a formal sp^2 hybrid, even considering the expected decrease caused by lone pair/lone pair repulsions. The values calculated here are also in agreement with those found in model systems, which will be discussed in the next section.

The VSCC of N(1) was also searched for (3,−3) critical points, and the results are shown in Table 9. As with the critical points associated with the oxygen atoms, the theoretical models

TABLE 6: Computed Atomic Charges (q, e), Dipoles (μ, D), and Lagrangians (au) from the Indicated Model[a]

	X AIM/HC	SCF AIM	PSCF AIM	MPSCF AIM/HC	DFT AIM	PDFT AIM	MPDFT AIM/HC
N(1)							
q	−0.16/−0.10	−0.12	−0.13	−0.13/0.03	−0.18	−0.16	−0.16/−0.05
$\|\mu\|$	1.46	2.03	2.05	1.90	1.78	1.83	1.64
L	8.8×10^{-4}	-4.7×10^{-4}	9.9×10^{-4}	1.2×10^{-3}	-4.4×10^{-4}	2.6×10^{-4}	5.8×10^{-4}
N(2)							
q	0.60/0.10	0.73	0.78	0.66/0.03	0.67	0.71	0.59/0.10
$\|\mu\|$	0.81	0.92	0.91	0.71	0.77	0.77	0.64
L	1.1×10^{-3}	-7.1×10^{-5}	3.2×10^{-3}	-7.9×10^{-4}	-1.1×10^{-4}	3.8×10^{-3}	-2.9×10^{-3}
N(3)							
q	0.66/0.12	0.76	0.82	0.69/0.05	0.69	0.74	0.62/0.11
$\|\mu\|$	0.53	0.95	0.91	0.77	0.79	0.77	0.69
L	3.9×10^{-4}	2.0×10^{-3}	-9.2×10^{-4}	2.8×10^{-3}	6.5×10^{-4}	-1.3×10^{-3}	1.3×10^{-3}
O(1)							
q	−0.46/−0.25	−0.59	−0.56	−0.52/−0.23	−0.55	−0.50	−0.46/−0.23
$\|\mu\|$	0.75	0.55	0.53	1.00	0.56	0.56	0.94
L	3.4×10^{-4}	-8.3×10^{-5}	1.5×10^{-4}	1.4×10^{-4}	-4.2×10^{-5}	-9.6×10^{-5}	1.5×10^{-4}
O(2)							
q	−0.54/−0.33	−0.59	−0.66	−0.56/−0.27	−0.55	−0.59	−0.50/−0.26
$\|\mu\|$	0.65	0.66	0.71	0.95	0.64	0.71	0.88
L	3.8×10^{-4}	9.2×10^{-5}	-1.3×10^{-4}	6.8×10^{-4}	1.1×10^{-4}	-3.0×10^{-4}	-3.5×10^{-4}
O(3)							
q	−0.54/−0.27	−0.60	−0.61	−0.54/−0.24	−0.55	−0.54	−0.48/−0.24
$\|\mu\|$	0.71	0.61	0.67	0.98	0.61	0.70	0.91
L	4.4×10^{-4}	7.5×10^{-5}	3.6×10^{-4}	3.4×10^{-4}	1.0×10^{-4}	2.1×10^{-4}	8.9×10^{-5}
O(4)							
q	−0.54/−0.30	−0.59	−0.60	−0.53/−0.24	−0.54	−0.54	−0.47/−0.23
$\|\mu\|$	0.74	0.56	0.65	0.99	0.57	0.68	0.92
L	3.5×10^{-4}	-2.7×10^{-4}	8.4×10^{-5}	-5.3×10^{-4}	-1.8×10^{-4}	8.5×10^{-5}	-4.5×10^{-4}
Sums							
q	−0.97	−1.00[b]	−0.95	−0.93/−0.87	−1.00[b]	−0.89	−0.87/−0.80
$\|L\|$	3.9×10^{-3}	3.0×10^{-3}	5.8×10^{-3}	6.4×10^{-3}	1.6×10^{-3}	6.1×10^{-3}	5.8×10^{-3}
Q_{tot}	0.0010[c]	−0.9997[d]	0.0031[c]	−0.0007[c]	−1.0003[d]	0.0025[c]	−0.0045[c]

[a] Summed quantities for the complete dinitramide ion are shown in the last row. HC, Hansen−Coppens, for abbreviations, see Table 1. [b] As computed in GAUSSIAN98. [c] The ammonium ion was integrated separately and its charge added to that of the dinitramide ion to obtain this number. [d] Integrated charge using AIM for the dinitramide ion.

TABLE 7: Comparison of Total Charges for Both Nitro Groups in the Dinitramide Ion

salt	model	$q(NO_2)$	O−N−N−N dihedral angle
ADN	X/MPDFT	−0.42/−0.33	27.9
		−0.40/−0.37	22.8
BIGH2	X	−0.46	23.1
		−0.54	9.5
BIGH	X	−0.43	4.2
		−0.05	2.8

closely reproduce experimental values of ρ_c at the (3,−3) critical points. Also, significant differences in values of $\nabla^2\rho_c$ are found that are again attributable to the lack of flexibility in the multipole fit, as shown by PSCF/MPSCF and PDFT/MPDFT comparisons. Experiment shows a single (3,−3) point that is significantly displaced from the NNN plane, as indicated by the dihedral angle of 142.9° formed with the NNN plane (see Table 9). The MPDFT model reproduces this result quite closely, giving a value of 147.8°. Furthermore, PDFT/MPDFT comparison shows that this large displacement from the NNN plane arises from the multipole fits. PDFT gives a value of 172.7°, which is the same as that found for a single molecular ion (close to the value of 180° expected for sp^2 hybridized nitrogen). The SCF results show different trends and will be discussed in more detail below.

Further information about the features of $-\nabla^2\rho(\mathbf{r})$ at N(1) can be found in Figure 5, which shows contour maps of this quantity in the plane bisecting the NNN angle, the nitro groups being at the top. In the right-hand panel, the experimental map is shown; at the left is the MPDFT map. Both of the maps show one minimum that lies in a large, relatively flat region in $\nabla^2\rho(\mathbf{r})$. This region was extensively searched for another minimum, but none was found.

The topology of the Laplacian around N(1) obtained with the SCF model differs from that found experimentally and with DFT. As in the DFT calculations and experiment, the SCF and PSCF models give only one (3,−3) critical point near N(1) and it makes a dihedral angle with the NNN plane of 165.5 and 162.7°, respectively. This angle differs from that found experimentally but is close to those found in DFT and PDFT models. However, the multipole fit (MPSCF) gives two critical points, each one of which is nearly ideally placed for conjugation of lone pairs with the nitro group, as indicated by the dihedral angles formed with the nitro group oxygens. This is clearly an artifact of the multipole fit; the "actual density" used to obtain the fit not possessing this topology.

However, location of the (3,−1) critical point linking the (3,−3) points at N(1) in the MPSCF density gives −65.2 e/Å^5 as the value for $\nabla^2\rho_c$, which is only slightly different from values of −67.2 and −68.4 e/Å^5 at the minima. This behavior is markedly different from that expected for two separate lone pairs, such as are found on the oxygen atoms. To further illustrate this point, some additional critical points in the VSCC of O(1) were located using the MPSCF model. As shown in Table 10, values of ρ_c and $\nabla^2\rho_c$ at these (3,−1) and (3,+1) VSCC critical points differ by factors of nearly 1.5 and over 2, respectively, from those found at the (3,−3) point (Table 8). So, although the SCF model gives two (3,−3) points suggesting two lone pairs at N(1), these do not exhibit the quantitative behavior expected of two lone pairs, but rather *a single broad continuous accumulation of electron density*.

TABLE 8: Properties of VSCC (3,−3) Critical Points in the Laplacian Associated with the Two Electron Lone Pairs Associated with the Oxygen Atoms of the Dinitramide Ion[a]

atom	ρ_c (e/Å^3)	$\nabla^2\rho_c$ (e/Å^5)	r (Å)	∠(lp−O−N), deg	D(lp−O−N−O), deg
O(1)					
X	6.76/6.41	−160.5/−150.9	0.335/0.338	114.6/99.6	−3.0/177.0
SCF	6.64/6.68	−103.0/−104.5	0.337/0.336	102.9/104.9	−2.3/178.2
PSCF	6.64/6.77	−103.5/−107.6	0.336/0.334	103.3/105.7	−3.1/178.2
MPSCF	6.80/6.85	−171.4/−173.3	0.334/0.333	100.3/102.8	−2.9/177.8
DFT	6.52/6.56	−93.8/−95.2	0.341/0.340	101.8/104.6	−2.9/177.8
PDFT	6.50/6.60	−94.4/−97.8	0.340/0.337	102.3/105.5	−3.7/178.0
MPDFT	6.73/6.78	−160.9/−163.6	0.334/0.333	99.3/102.6	−3.5/177.8
O(2)					
X	6.68/6.75	−152.5/−160.3	0.336/0.335	100.4/94.1	−0.7/167.6
SCF	6.64/6.65	−103.5/−103.9	0.337/0.337	102.6/102.8	−1.4/179.1
PSCF	6.36/6.32	−94.4/−93.4	0.343/0.344	104.1/104.6	−2.9/178.8
MPSCF	6.63/6.62	−160.9/−159.6	0.336/0.336	102.2/102.8	−3.1/179.1
DFT	6.58/6.59	−96.3/−96.5	0.340/0.339	101.5/102.3	−1.6/178.9
PDFT	6.22/6.19	−86.4/−85.4	0.346/0.347	103.6/104.8	−3.0/179.0
MPDFT	6.56/6.55	−151.9/−150.8	0.336/0.336	102.3/103.7	−3.2/179.3
O(3)					
X	6.34/6.41	−141.8/−142.8	0.339/0.339	107.4/111.3	−12.0/157.6
SCF	6.65/6.67	−103.6/−104.0	0.337/0.337	103.4/103.1	−1.7/178.9
PSCF	6.65/6.44	−103.5/−97.0	0.336/0.342	105.4/103.5	−1.7/179.0
MPSCF	6.79/6.71	−169.4/−166.6	0.334/0.335	103.5/101.2	−1.7/179.0
DFT	6.57/6.59	−95.7/−96.0	0.340/0.340	102.3/102.5	−2.0/178.5
PDFT	6.54/6.29	−95.6/−88.3	0.339/0.345	104.9/103.0	−1.7/179.0
MPDFT	6.74/6.63	−161.1/−157.0	0.334/0.335	103.6/101.1	−1.6/178.5
O(4)					
X	6.36/6.55	−137.2/−149.5	0.339/0.337	93.2/111.6	0.0/−159.6
SCF	6.64/6.69	−103.3/−105.0	0.337/0.336	103.3/104.2	−2.5/178.0
PSCF	6.53/6.76	−98.9/−106.7	0.339/0.334	103.4/104.8	−3.9/177.6
MPSCF	6.74/6.87	−167.2/−174.1	0.334/0.333	100.9/101.9	−3.0/177.1
DFT	6.54/6.59	−94.6/−96.2	0.340/0.339	102.1/103.9	−2.9/177.4
PDFT	6.39/6.64	−90.2/−98.3	0.342/0.337	101.9/104.6	−5.0/177.0
MPDFT	6.67/6.83	−157.6/−166.0	0.334/0.333	99.7/101.9	−3.7/176.6

[a] "lp" represents a (3,−3) VSCC critical point associated with a lone pair of electrons. For abbreviations, see Table 1.

TABLE 9: VSCC (3,−3) Critical Points and a (3,−1) Critical Point in the Laplacian Associated with the Electron Lone Pair on the Central Nitrogen of Dinitramide Ion from the Different Models[a]

model	ρ_c (e/Å^3)	$\nabla^2\rho_c$ (e/Å^5)	r (Å)	angle (dihedral angle), deg[b]
N(1)				
(3,−3) cp				
X	3.61	−64.0	0.399	122.8(142.9)
SCF	3.73	−50.0	0.394	121.8(165.5)
PSCF	3.73	−49.8	0.392	121.0(162.7)
MPSCF	3.65/3.68	−67.2/−68.4	0.398/0.398	111.6/109.9 (−122.8/129.1) dihedral:[c] 96.7/106.3 O(4)/O(1)
(3,−1) cp				
	3.63	−65.2	0.400	123.3(−170.9)
(3,−3) cp				
DFT	3.71	−46.4	0.396	122.9(172.7)
PDFT	3.69	−46.2	0.395	122.6(172.7)
MPDFT	3.66	−65.8	0.398	118.1(147.8)

[a] For abbreviations, see Table 1. [b] Refers to lp−N(1)−N(2) angle and lp−N(1)−N(2)−N(3) dihedral angle. [c] Refers to lp−N−N−O_{inner} dihedral angle.

One final point concerns the dihedral angle formed by the (3,−3) critical point in the Laplacian at N(1) with the NNN plane. Figure 6 shows the location of the three hydrogen atoms nearest to N(1); the location of the critical point from the experimental data is also shown by the red-dashed line. It can be seen that H(2) and H(4) are ideally situated to contribute to the description of the N(1) lone pair. The more pronounced minimum in $\nabla^2\rho(\mathbf{r})$ at N(1) from the experimental data is also consistent with the lower κ' value for hydrogen in the X refinement; this leads to a more diffuse charge distribution. The

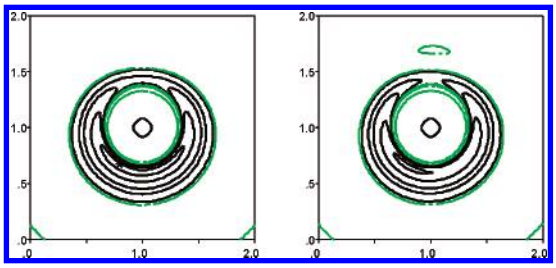

Figure 5. Some values of $-\nabla^2\rho(\mathbf{r})$ in the plane bisecting the N−N−N angle. This plane contains only the central nitrogen of the dinitramide ion in ammonium dinitramide: theoretical map (MPDFT) at left, experimental map (X) at right. The green line is 0.0; black lines represent contour values of 1, 10, 20, 40, and 60 e/Å.[5] The approximate position of the (3,−3) critical point in the MPDFT map is shown by the "*".

TABLE 10: Values of Topological Parameters at Some VSCC Critical Points near O(1) from MPSCF, To Be Compared with the Values for the (3,−3) Point at N(1) Shown in Table 9

atom/type	ρ_c (e/Å^3)	$\nabla^2\rho_c$ (e/Å^5)	r (Å)	∠(lp−O−N)	D(lp−O−N−O)
O(1)					
type					
(3,−1)	5.19/5.27	−75.6/−79.4	0.355/0.354	105.6/110.2	86.4/−91.5
(3,+1)	4.60	−33.2	0.368	177.4	58.6

modeling indicates that the (3,−3) point in the real crystal is nearer the location given by the PDFT model.

Although quantitative differences exist between theory and experiment in the description of the $-\nabla^2\rho(\mathbf{r})$ field, there is uniform agreement that the central nitrogen is better described as sp^2 hybridized as it does not have the two lone pairs required for sp^3 hybridization. A similar result was obtained for the BIGH

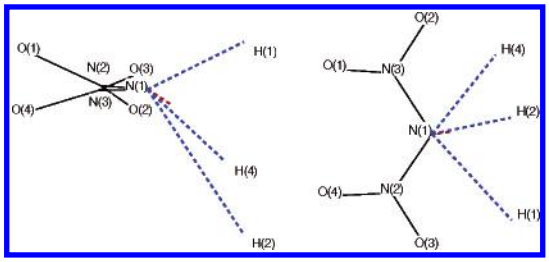

Figure 6. Two views showing the locations of the lone pair on the central nitrogen (red) and the nearest hydrogens in the ammonium dinitramide crystal. The lone pair location is from experimental data (X).

and BIGH2 salts and the robustness of the topology of the charge density and the Laplacian of the dinitramide ion is thereby confirmed.

F. Hybridization of the Nitro Group Oxygen. As shown in Table 8, some of the (3,−3) critical points in the $-\nabla^2\rho(\mathbf{r})$ VSCC occur near the oxygens of nitro groups, where lone pairs of electrons are expected. The angles formed by such critical points with the N−O bond are of interest, as they are related to the hybridization of the oxygen atom. Values of $-\nabla^2\rho(\mathbf{r})$ at such critical points are also of interest as they give quantitative information about the degree of charge concentration in these regions. Table 8 summarized the locations and properties of these points in the dinitramide ion, both as a single molecular ion and in the ammonium dinitramide crystal. The DFT model gives a range of lp−O−N angles of 101.5−104.6°, whereas PDFT gives 102.3−105.5°. The robustness of the Laplacian topology is demonstrated by the close overlap of these ranges.

To interpret these values further, B3LYP/6-21G** calculations and AIM analyses were performed for some prototypical systems resembling dinitramide. The results are shown in Table 11. The lp−O−N angles involving oxygen in nitro groups are found to be within the same range of those in dinitramide. Nitrite ion gives evidence of a canting of the lone pairs, which maintains the lp−O−lp angle (155°) very near the value of 156.2° found in nitrate ion. Similar values of this angle are found in nitromethane (154.6°) and the nitromethide ion (156.8°). Values of ρ_c and $\nabla^2\rho_c$ in nitrite and nitrate are also similar to those in dinitramide and to a lesser extent in the nitromethide ion. But, in nitromethane, values of ρ_c and $\nabla^2\rho_c$ show greater charge concentration.

The values discussed above can be compared with those found in formaldehyde and urea, which have a carbonyl oxygen. In these molecules, the lp−O−N angle is larger than found in nitro groups. The angle between the lone pairs has closed to 140.2 and 137.8°, respectively. In formaldehyde, values of ρ_c and $\nabla^2\rho_c$ are slightly larger in magnitude than those found in dinitramide, whereas significantly smaller values are found in urea.

Thus, the computational data for nitrite, nitrate, and nitromethide lone pair regions, show striking similarities to that for dinitramide. Although there are significant differences found when the carbonyl oxygens of formaldehyde and urea are considered, there is a qualitative similarity in the location of the critical points. Consequently, we find the (3,−3) critical points at oxygen on nitro groups are representative of slightly more sp-like hybridization than that found for the carbonyl groups in formaldehyde or urea. Nonetheless, the similarities between the (3,−3) critical points at oxygens in dinitramide and formaldehyde indicate the presence of electron lone pairs that are very similar in nature. This contrasts with some recent findings in N_2O_4.[8] It is noteworthy that the presence of a negative charge on dinitramide (or nitromethide) does not alter the apparent hybridization of the nitro group oxygen.

G. Volume of Dinitramide. The AIM theory allows partitioning of the molecular electron density into atomic contributions. The volumes enclosed by the zero flux partitioning surfaces can be obtained from computations and experiment, and resulting values are shown in Table 12. Ratios of the unit cell volume obtained from adding atomic volumes to that obtained from the experimental unit cell constants ranges from 0.998 to 1.000. Computed atomic volumes are sometimes larger and sometimes smaller compared with experiment but are in close agreement. The volume of the ammonium ion is larger and that of the dinitramide ion is smaller in the calculations than that obtained from experiment. Discrepancies due to effects of the multipole fit are small, as comparison of computed volumes and enclosed electron populations from the periodic and multipole models show good agreement. However, volume changes attributable to incorporation of the molecule into the crystal lattice are smaller in many cases than the PSCF/MPSCF and PDFT/MPDFT differences.

It is of interest to compare the AIM volumes of the dinitramide ion in its salts, BIGH, BIGH2, and ADN (Table 12). Total volumes of the dinitramide ion from experiment are 87.19, 84.66, and 85.10 Å^3, respectively. Atomic volumes found in the BIGH and BIGH2 salts for N(1) are 12.86 and 12.52 Å^3 compared with a value of 13.23 in ADN; nitro group nitrogens range from 6.02 to 6.36, compared with 5.95 and 6.55 Å^3; oxygens range over 14.39−17.09 Å^3, compared with the range 14.03−15.45 Å^3. Although the total dinitramide ion volume in ADN is between that found in BIGH and BIGH2, atomic volumes do not always lie within their corresponding ranges. Hence, there is a compensation in the changes among the atomic volumes. This is occurring despite the differences of charge transfer found in the three different salts.

H. Dipole Moment of the Dinitramide Ion. AIM partitions the crystal electron density into atomic regions that enclose all of the nuclei of the dinitramide ion. Integration of $\rho(\mathbf{r})$ over these regions gives the molecular dipole moment in the crystal, shown for the *x*-component, as follows:

$$\mu_x = \int_\Omega x_{\mathrm{mol}}\rho(\mathbf{r})\,\mathrm{d}\mathbf{r} \tag{4}$$

where the integral is taken over the volume bounded by the zero flux surfaces for the dinitramide ion. After partitioning the molecule into atoms, the integration may be replaced with a sum of integrals, each over an atomic basin, and the molecular *x*-coordinate is replaced with its value in each atomic frame, $x_{\mathrm{mol}} = x + x_{\mathrm{atom}}$, where the unsubscripted *x* is now with respect to each atomic center and is the variable of integration. Then

$$\mu_x = \Sigma_{\mathrm{atoms}}\{x_{\mathrm{atom}}\int_\Omega \rho(\mathbf{r})\,\mathrm{d}\mathbf{r} + \int_\Omega x\rho(\mathbf{r})\,\mathrm{d}\mathbf{r}\} \tag{5}$$

and

$$\mu_x = \Sigma_{\mathrm{atoms}}\{x_{\mathrm{atom}}q_{\mathrm{atom}} + \mu_{\mathrm{x,atom}}\} \tag{6}$$

Similar equations can be written for the other dipole components. Equation 6 makes it clear that the molecular dipole is the sum of two contributions. One is the product of an atomic coordinate and an atomic charge; the other is an atomic dipole referenced to the atom as origin. In this work, contributions from the first term on the right-hand side of eq 6 are called "atomic charge dipoles"; contributions from the second term are called "atomic dipoles". The term "total dipole" is used to mean the dipole that is the sum of the atomic charge dipoles and atomic dipoles. Also, eq 6 makes it clear that the total dipole moment and the charge dipoles of a charged species are both

TABLE 11: Properties Associated with Some (3,−3) Critical Points in the Laplacian That Are Associated with Electron Lone Pairs (lp) on Oxygen[a]

molecule/ion	ρ_c (e/Å^3)	$\nabla^2\rho_c$ (e/Å^5)	r_c (Å)	∠(lp−O−N), deg	D(lp−O−X−Y), deg
nitrite (NO_2^-)	6.58	−97.2	0.341	99.5	180.0[b]
	6.56	−96.0	0.341	105.5	0.0[b]
nitrate (NO_3^-)	6.52	−94.1	0.341	101.9	0.0/180.0[b]
nitromethane (CH_3NO_2)	6.76	−103.0	0.334	104.2	0.0[b]
	6.74	−102.3	0.336	101.2	−179.8[b]
nitromethide ($CH_2NO_2^-$)	6.41	−91.0	0.344	101.8	0.0[b]
	6.37	−90.2	0.345	101.4	180.0[b]
formaldehyde (CH_2O)	6.60	−97.3	0.337	109.9	0.0,[c] 180.0[c]
urea ($CO(NH_2)_2$)	5.98	−77.4	0.352	111.1	0.0/180.0[d]
DN	6.52−6.59	−93.8 to −96.5	0.339−0.341	101.5−104.6	−1.6 to −2.9/177.4−178.9[b]

[a] Results were obtained for a single molecule that had been energy optimized using the DFT method. [b] X = N, Y = O. [c] X = C, Y = H. [d] X = C, Y = N.

TABLE 12: Computed Volumes and Enclosed Electron Populations[a]

	V_{tot} (Å^3)	$V_{0.001}$ (Å^3)	$N_{0.001}$ (e)	$V_{0.002}$ (Å^3)	$N_{0.002}$ (e)		V_{tot} (Å^3)	$V_{0.001}$ (Å^3)	$N_{0.001}$ (e)	$V_{0.002}$ (Å^3)	$N_{0.002}$ (e)
N(1)						O(3)					
X	13.23	12.39	7.16	11.67	7.15	X	14.78	14.45	8.53	13.44	8.52
SCF		13.15	7.11	11.61	7.09	SCF		14.44	8.58	12.31	8.56
PSCF	13.62	12.98	7.13	11.91	7.12	PSCF	14.64	14.14	8.61	12.96	8.59
MPSCF	13.21	13.09	7.13	12.28	7.12	MPSCF	14.65	14.65	8.54	14.20	8.53
DFT		13.24	7.17	11.09	7.15	DFT		13.96	8.53	11.96	8.51
PDFT	13.46	12.88	7.16	11.81	7.15	PDFT	14.45	14.01	8.54	12.88	8.53
MPDFT	13.04	12.90	7.16	12.07	7.15	MPDFT	14.39	14.39	8.48	13.91	8.47
N(2)						O(4)					
X	6.55	6.53	6.40	6.29	6.40	X	14.03	13.63	8.53	12.98	8.53
SCF		5.97	6.27	5.59	6.22	SCF		13.95	8.57	12.05	8.55
PSCF	6.04	5.89	6.22	5.59	6.22	PSCF	14.03	13.71	8.60	12.85	8.59
MPSCF	6.15	6.15	6.34	6.04	6.34	MPSCF	14.07	14.07	8.53	13.73	8.53
DFT		6.17	6.32	5.76	6.32	DFT		13.60	8.52	11.80	8.50
PDFT	6.29	6.15	6.29	5.82	6.29	PDFT	13.89	13.63	8.54	12.79	8.53
MPDFT	6.67	6.67	6.41	6.44	6.41	MPDFT	13.80	13.80	8.47	13.47	8.47
N(3)						$N_3O_4^-$					
X	5.95	5.95	6.34	5.91	6.34	X	85.10	81.71	53.96	77.19	53.92
SCF		5.91	6.24	5.50	6.24	SCF		81.85	53.90	71.47	53.80
PSCF	5.66	5.62	6.18	5.53	6.18	PSCF	84.29	81.40	53.93	75.04	53.87
MPSCF	5.74	5.74	6.31	5.74	6.31	MPSCF	84.61	84.35	53.93	80.95	53.89
DFT		6.14	6.30	5.74	6.30	DFT		80.70	53.90	70.17	53.79
PDFT	5.94	5.90	6.26	5.76	6.25	PDFT	83.99	81.52	53.88	75.21	53.82
MPDFT	6.07	6.07	6.38	6.05	6.38	MPDFT	84.13	83.86	53.87	80.30	53.83
O(1)						NH_4^+					
X	15.45	14.31	8.46	13.34	8.45	X	24.73	22.57	10.03	21.12	10.02
SCF		13.93	8.57	12.04	8.56	SCF		28.74	9.93	23.16	9.88
PSCF	15.11	14.42	8.55	13.00	8.54	PSCF	25.62	24.58	10.04	22.67	10.02
MPSCF	15.43	15.32	8.52	14.49	8.51	MPSCF	25.32	24.93	10.07	23.41	10.05
DFT		13.58	8.53	11.81	8.51	DFT		29.02	9.93	23.19	9.87
PDFT	14.94	14.35	8.50	12.92	8.48	PDFT	25.97	25.12	10.10	23.16	10.08
MPDFT	15.19	15.06	8.46	14.23	8.46	MPDFT	25.96	25.54	10.13	24.01	10.11
O(2)						Unit Cell					
X	15.11	14.46	8.54	13.56	8.53	X	439.3	417.1	255.98	373.2	255.74
SCF		14.50	8.57	12.40	8.55	SCF		442.4	255.32	378.5	254.68
PSCF	15.19	14.64	8.65	13.22	8.64	PSCF	439.7	424.0	255.91	390.9	255.58
MPSCF	15.35	15.34	8.56	14.47	8.55	MPSCF	439.7	437.1	255.99	417.4	255.77
DFT		14.02	8.53	12.01	8.50	DFT		438.9	255.32	373.4	254.64
PDFT	15.02	14.60	8.59	13.22	8.58	PDFT	439.8	426.5	255.92	393.5	255.59
MPDFT	14.98	14.98	8.50	14.12	8.49	MPDFT	440.3	437.6	256.00	417.3	255.78

[a] The unit cell volume is 440.20 Å^3 and total electron population is 256 e. For abbreviations, see Table 1. Subscripts for V and N refer to 0.001 and 0.002 au surfaces, respectively.

origin dependent in contrast to neutral systems (where substitution of $x_{atom} = x_{atom} + x_{translation}$ gives an $x_{translation}\Sigma q_{atom}$ term, which is zero). In all results herein, the total molecular dipole moments are with respect to the center of mass of the dinitramide ion. Because the calculations were all performed at the same geometry, this permits a comparison between the moments obtained from different models. Atomic dipoles are always with respect to the nucleus.

Computed atomic dipole moment magnitudes are given in Table 6, and the total dipole moments in Table 13. AIM analysis of charge demonstrates several effects of the crystal lattice and of the models. The SCF and DFT results for the total dipole moment for a single molecular anion of 0.49 and 0.44 D, respectively, are in close agreement. A value of 0.69 D is found from the experimental data with the AIM analysis, giving an enhancement factor of 1.41. Similar SCF/MPSCF and DFT/MPDFT comparisons give enhancement factors of 0.96 and 1.02; i.e., the enhancement essentially disappears. These MPSCF/MPDFT derived moments, however, are shown to be too small by PSCF/MPSCF and PDFT/MPDFT comparisons: the "in-crystal" dipole moment (PSCF/PDFT) obtained is 1.12 and 1.08 D, respectively, giving enhancement factors of 2.3 and 2.5

TABLE 13: Components of the Total Dipole Moment (D) for the Dinitramide Ion in the Inertial Frame[a]

	$\mu_{tot,x}$	$\mu_{tot,y}$	$\mu_{tot,z}$	$\lvert\mu_{tot}\rvert$
X	−0.07	−0.08	0.68	0.69
SCF	0.29	0.39	0.02	0.49
PSCF	0.71	0.86	0.11	1.12
MPSCF	0.47	−0.05	0.04	0.47
DFT	0.24	0.37	0.01	0.44
PDFT	0.70	0.82	0.10	1.08
MPDFT	0.44	−0.05	0.01	0.45

[a] For abbreviations, see Table 1.

with respect to the single molecule. Thus, the multipole fitting procedure leads to significant underestimation in the determination of the "in-crystal" dipole moment. Further evidence of this is found when the total molecular dipole is computed from the fitted multipole populations alone. In all three cases, there is a small diminution of the dipole magnitude, not an enhancement!

There is also a very large difference between experiment and theory in the direction of the "in-crystal" dipole. The computational results show the dipole components are principally in the *xy* plane whereas the experimental result is nearly perpendicular. As a result of the difference between theory and experiment, additional analysis of the components was performed.

Further information about the genesis of the molecular dipole moment is shown in Figure 7. It shows projections of the molecular and atomic dipoles of both an isolated dinitramide ion and one in the ammonium dinitramide crystal. The figure shows only results from the X, PDFT, and MPDFT models, the SCF results being quite similar. Changes in the molecular dipole moment that accompany incorporation of a single dinitramide ion into the ammonium dinitramide lattice are of particular interest. Figure 7 illustrates these changes graphically. We believe that the PDFT result is the most realistic, as it is obtained from a wave function analysis and is not subject to any limitations of the multipole fitting procedure. As can be observed in the PDFT drawing in Figure 7, the sums of the atomic charge dipoles and atomic dipoles (shown in red and green, respectively, near the center of each drawing) are oriented in nearly opposite directions in the single molecule and the crystal. Upon incorporation into the crystal, the sum of the atomic dipole contributions as well as each individual atomic dipole remain almost constant, each term being alike in both direction and magnitude. The total dipole enhancement is found to arise principally from changes in the atomic charge dipoles. This is evident when the solid and dashed red arrows near the center of the PDFT drawing are compared. Although the magnitude of the isolated molecule and "in-crystal" total atomic charge dipole (red) is similar, the angle between this vector and the total atomic dipole (green) contribution has changed; i.e., the atomic charge vector has been rotated by the crystal environment. The result is an enhancement of the total molecular dipole (blue) by a factor much larger than the increase in magnitude of any of the individual components. Further, this rotation is directly related to changes in atomic charges upon incorporation into the crystal lattice, as shown by the PDFT results in Table 6 (O(2) gained charge, whereas the other oxygens lost charge or remained the same). Inspection of the results in Table 5 shows that O(2) has two strong hydrogen bonds, whereas the other oxygens have fewer. Therefore, the rotation of the charge dipole moment may arise from strong asymmetric hydrogen bonding in the crystal. This occurs while the overall molecular charge topology and individual atomic dipoles remain nearly constant.

Figure 7 also shows changes in the dipoles with respect to the DFT calculations given by an analysis of experimental data and from the MPDFT model. There are significant changes evidenced in a PDFT/MPDFT comparison. Most significantly, in the MPDFT result, the atomic dipoles (green) do not to show the same degree of additivity found in the PDFT result. This is clearly a shortcoming of the multipole fit procedure, as the PDFT/MPDFT models are based on the same underlying charge distribution.

The X results in Figure 7 show features similar to those observed in the MPDFT model; in particular, the sum of the atomic dipoles are significantly less than in the PDFT model. Although the resulting dipole moment enhancement found from the experimental data is significant, it is not as large as that found in the PDFT model. It is also pointed in a direction nearly perpendicular to that obtained from the PDFT result. Nevertheless, the PDFT result is preferred because the X/MPDFT comparison shows similarities that are most likely to be the result of limitations of the multipole fit procedure.

Discussion and Conclusions

A clear and consistent picture of the dinitramide ion in its salts has emerged: the molecular charge topology and that of the Laplacian is quite robust with respect to different models. The O···O atomic interaction line is found to have very similar properties both in a single molecule and in the crystal, when the crystal data are available. This leads to the prediction that the O···O AIL should be observed in salts not yet characterized, when the single molecule at the crystal geometry shows this feature. Lone pairs of electrons near oxygens are found at similar positions in the single molecule and in the crystal. In addition, a single extended lone pair of electrons at N(1), previously observed in BIGH and BIGH2 salts, is found in ADN. It is likewise found in single molecule calculations at the crystal geometry. This leads to the prediction that it is also a robust feature of the ion and should be observed in other salts when the single molecule at the crystal geometry shows a single lone pair. The consistent compression of the NNN angle to <120° found in crystal structures is thus, in agreement with VSEPR theory, the result of lone pair/bond-pair electron repulsions.

It is important to place some limits on the robustness of the topology of the electron density in the dinitramide ion. In the C_{2v} conformation in which the nitro groups are twisted to minimize conjugation, it seems unlikely that the AIL between oxygens would be present—the distance between the "inner oxygens" would be too long. In addition, the dinitramide rhenium complex shows one of the nitro groups is twisted by approximately 60°.[1d] This value is much larger than that found in any of the dinitramide salts.[1] The rhenium complex is also the only instance of a transition metal coordination complex with dinitramide ion. Differences in the nature of the bonding interactions with the dinitramide ion in this complex may change the charge topology of the dinitramide moiety. Except for the rhenium complex, in all other structurally characterized salts the dinitramide anions are found to lie very close in energy.[1] We expect the charge topology of the dinitramide ion to remain unchanged in this region. Finally, we use the term robust to indicate a high degree of similarity in the features of the charge density distribution and its Laplacian at a similar molecular geometry. We do not expect these features to be identical in different environments. Indeed, it is a subject of interest to discover how the environment does affect the Laplacian; but we have placed some limits on the size of the changes that can be expected.

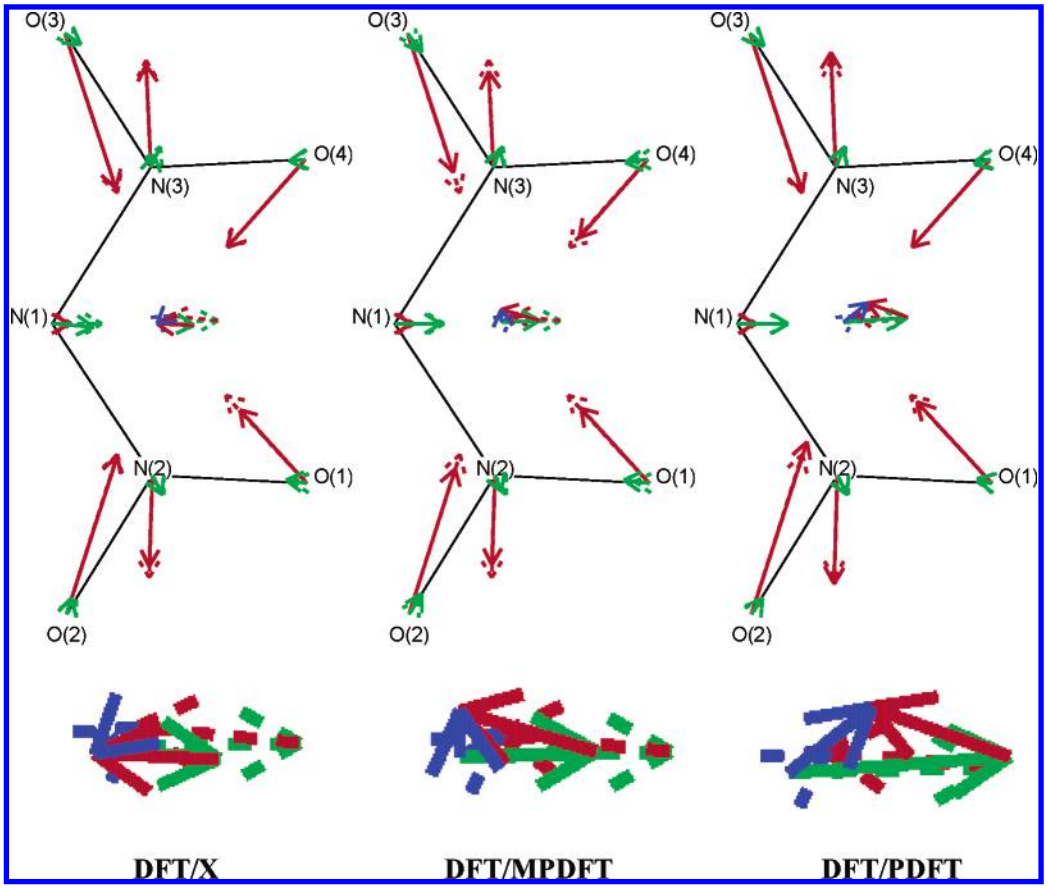

Figure 7. Projected atomic and molecular dipole moments for the isolated dinitramide ion and in ammonium dinitramide. Molecular dipole moments from the DFT calculations are shown as dashed lines; they are the same in all three drawings. Dipole moments of the ion in the crystal are shown as colored solid lines. Molecular dipole components are shown with the center of mass as origin, which is near the center of each drawing, and are enlarged ×3 below. Atomic dipole components are shown with the nucleus as origin. The total molecular dipole moment is shown in blue, and the two components shown in red (charge dipole) and green (dipole). Atomic contributions to these sums are colored similarly. In many cases a dashed line is not visible because a solid line overlays it, but its presence is indicated by its arrowhead when the projections are not of equal length. All dipoles point from negative to positive. The *xy* plane in the inertial frame of the dinitramide ion is shown. The largest components of some of the dipoles in the X model are along the *z*-axis and are not visible in this figure (see Table 13).

Given the robustness of the charge topology, one may ask how can a dipole moment enhancement in the crystal occur? The theoretical calculations give a clear picture free of effects found in the multipole fitting procedure. These effects can exaggerate the dipole moments derived from experimental data.[33] In ADN, it is found that the largest charge buildup is on the oxygen that has the most hydrogen bonds. The presence of such strong hydrogen bonds is frequently associated with significant crystal-induced dipole moments[34] but is not required.[9a] Decomposition of the molecular dipole moment into atomic charge and atomic dipole components (see eq 6) using AIM shows that the atomic dipole contribution remains of approximately the same magnitude and direction in both the crystal and single molecule. It is another robust feature of the charge topology. The atomic charge dipoles, however, behave differently and are principally responsible for the dipole moment enhancement found in the PDFT model.

AIM has provided a useful means of analyzing the charge densities modeled in this work. Because AIM derives from the principle of stationary action and the identification of regions over which $\int \nabla^2 \rho(\mathbf{r}) = 0$ that enclose a single nucleus, it is unbiased by arbitrary assumptions about the underlying charge distribution. Our results offer further evidence that AIM can identify "chemical" features of the electron density. Nonetheless, the AIL's between the "inner" oxygens indicate a charge topology the same as that found in ionic interactions, in hydrogen bonds, and in rare-gas dimers. They are also found in the equilibrium structures of several dinitramide salts and are, consequently, quite robust. But, such AIL's are not expected if the separation between oxygens becomes too large for sufficient overlap. In salts, the range of the nitro group rotations remains in a region where the formal charge on the central nitrogen can be effectively delocalized.[1a] If the nitro group rotations increase the O···O separation significantly beyond that found in known salts, the AIL is not likely to appear. The rhenium coordination compound is such an example.[1d]

Acknowledgment. We thank the Office of Naval Research for financial support through contract number N00014-95-1-0013, Dr. A. Volkov and Prof. P. Coppens who made the TOPXD program available to us, Yu.-Sh. Chen for providing valuable assistance with computers and software, and Dr. K. Kirschbaum for helpful discussions.

Supporting Information Available: Deformation density maps, Laplacian maps, refined coordinates, and multipole population parameters are available as Supporting Information. This material is available free of charge via the Internet at http://pubs.acs.org.

References and Notes

(1) (a) Pinkerton, A. A.; Ritchie, J. P. *J. Mol. Struct.* **2003**, *657*, 57. (b) Gilardi, R.; Flippen-Anderson, J.; George, C.; Butcher, R. J. *J. Am. Chem. Soc.* **1997**, *119*, 9411. (c) Martin, A.; Pinkerton, A. S.; Gilardi, R.

D.; Bottaro, J. C. *Acta Crystallogr.* **1997**, *B53*, 504. (d) Trammell, S.; Goodson, P. A.; Sullivan, B. P. *Inorg. Chem.* **1996**, *35*, 1421. (e) Gilardi, R.; Butcher, R. J. *J. Chem. Crystallogr.* **2000**, *30*, 599. (f) Butcher, R. J.; Gilardi, R. D. *J. Chem. Crystallogr.* **1998**, *28*, 95. (g) Gilardi, R. D.; Butcher, R. J. *J. Chem. Crystallogr.* **1998**, *28*, 105. (h) Gilardi, R. D.; Butcher, R. J. *J. Chem. Crystallogr.* **1998**, *28*, 163. (i) Gilardi, R. D.; Butcher, R. J. *J. Chem. Crystallogr.* **1998**, *28*, 673. (j) Tanbug, R.; Kirschbaum, K.; Pinkerton, A. A. *J. Chem. Crystallogr.* **1999**, *29*, 25. (k) Sitzmann, M. E.; Gilardi, R.; Butcher, R. J.; Koppes, W. M.; Stern, A. G.; Thrasher, J. S.; Trivedi, N. J.; Yang, Z.-Y. *Inorg. Chem.* **2000**, *39*, 843. (l) Dubovitskii, F. I.; Golovina, N. I.; Pavlov, A. N.; Atovmyan, L. O. *Proc. Nat. Acad. Sci. U.S.S.R.* **1998**, *360*, 491. (m) Gilardi, R.; Butcher, R. J. *J. Chem. Crystallogr.* **2002**, *32*, 477. (n) Romanenko, G. V.; Varand, V. L.; Podberezskaya, N. V.; Naumov, D. Yu.; Gromilov, S. A.; Larionov, S. V. *Russ. J. Struct. Chem.* **2001**, *42*, 1233.

(2) Shlyapochnikov, V. A.; Tafipolsky, M. A.; Tokmakov, I. V.; Baskir, E. S.; Anikin, O. V.; Strelenko, Yu. A.; Luk'yanov, O. A.; Tartakovsky, V. A. *J. Mol. Struct.* **2001**, *559*, 147.

(3) Bader, R. F. W. *Atoms in Molecules: A Quantum Theory*; Clarendon Press: Oxford, 1990.

(4) (a) Zhurova, E. A.; Tsirelson, V. G.; Stash, A. I.; Pinkerton, A. A. *J. Am. Chem. Soc.* **2002**, *124*, 4574. (b) Zhurova, E. A.; Martin, A.; Pinkerton, A. *J. Am. Chem. Soc.* **2002**, *124*, 8741.

(5) (a) Bader, R. F. W. *J. Phys. Chem.* **1998**, *A102*, 7314. (b) Cioslowski, J.; Edgington, L.; Stefanov, B. B. *J. Am. Chem. Soc.* **1995**, *117*, 10381. (c) Bachrach, S. M. *J. Am. Chem. Soc.* **1986**, *108*, 6406.

(6) Politzer, P.; Seminario, J. M.; Concha, M. C.; Redfern, P. C. *J. Mol. Struct. (THEOCHEM)* **1993**, *287*, 235.

(7) McMurry, J.; Fay, R. C. *Chemistry*, 2nd ed.; Prentice Hall: Upper Saddle River, NJ, 1998.

(8) Messerschmidt, M.; Wagner, A.; Wong, M. W.; Luger, P. *J. Am. Chem. Soc.* **2002**, *124*, 732.

(9) (a) May, E.; Destro, R.; Gatti, C. *J. Am. Chem. Soc.* **2001**, *123*, 12248. (b) Volkov, A.; Gatti, C.; Abramov, Y.; Coppens, P. *Acta Crystallogr.* **2000**, *A56*, 252. (c) Abramov, Yu. A.; Volkov, A.; Coppens, P. *J. Mol. Struct. THEOCHEM.* **2000**, *529*, 27.

(10) Spackman, M. A. *Chem. Rev.* **1992**, *92*, 1769.

(11) Gatti, C.; Saunders, V. R.; Roetti, C. *J. Chem. Phys.* **1994**, *101*, 10686.

(12) Zhang, Y.; Coppens, P. *Chem. Commun.* **1999**, 2425.

(13) Coppens, P. *X-ray Charge Densities and Chemical Bonding*; International Union of Crystallography, Oxford Press: Oxford, U.K., 1997.

(14) Baert, F.; Coppens, P.; Stevens, E. D.; DeVos, L. *Acta Crystallogr.* **1982**, *A38*, 143.

(15) Hansen, N. K.; Coppens, P. *Acta Crystallogr.* **1978**, *A34*, 909.

(16) (a) Volkov, A.; Coppens, P. *Acta Crystallogr.* **2001**, *A57*, 395 and reference therein. (b) Bianchi, R.; Gatti, C.; Adovasio, V.; Nardelli, M. *Acta Crystallogr.* **1996**, *B52*, 471. (c) Volkov, A.; Abramov, Y.; Coppens, P.; Gatti, C. *Acta Crystallogr.* **2000**, *A56*, 332 and references therein. (d) Bytheway, I.; Chandler, G. S.; Figgis, B. N. *Acta Crystallogr.* **2002**, *A58*, 451.

(17) *Fundamentals of Crystallography*; Giacovazzo, C., Ed.; Oxford University Press: New York, 1998.

(18) Hehre, W. J.; Radom, L.; Schleyer, P. v. R.; Pople, J. A. *Ab Initio Molecular Orbital Theory*; Wiley-Interscience: New York, 1986 (see also references therein).

(19) Frisch, M. J.; Trucks, G. W.; Schlegel, H. B.; Scuseria, G. E.; Robb, M. A.; Cheeseman, J. R.; Zakrzewski, V. G.; Montgomery, J. A., Jr.; Stratmann, R. E.; Burant, J. C.; Dapprich, S.; Millam, J. M.; Daniels, A. D.; Kudin, K. N.; Strain, M. C.; Farkas, O.; Tomasi, J.; Barone, V.; Cossi, M.; Cammi, R.; Mennucci, B.; Pomelli, C.; Adamo, C.; Clifford, S.; Ochterski, J.; Petersson, G. A.; Ayala, P. Y.; Cui, Q.; Morokuma, K.; Malick, D. K.; Rabuck, A. D.; Raghavachari, K.; Foresman, J. B.; Cioslowski, J.; Ortiz, J. V.; Baboul, A. G.; Stefanov, B. B.; Liu, G.; Liashenko, A.; Piskorz, P.; Komaromi, I.; Gomperts, R.; Martin, R. L.; Fox, D. J.; Keith, T.; Al-Laham, M. A.; Peng, C. Y.; Nanayakkara, A.; Challacombe, M.; Gill, P. M. W.; Johnson, B.; Chen, W.; Wong, M. W.; Andres, J. L.; Gonzalez, C.; Head-Gordon, M.; Replogle, E. S.; Pople, J. A. *Gaussian 98*, revision A.9; Gaussian, Inc.: Pittsburgh, PA, 1998.

(20) (a) Becke, A. D. *J. Chem. Phys.* **1993**, *98*, 5648. (b) Lee, C.; Yang, W.; Parr, R. G. *Phys. Rev.* **1988**, *B37*, 785.

(21) (a) AIMPAC programs: Bubble 2.0, PROAIMV−Version 94−Revision B, Extreme were used. (b) Biegler-Konig, F. W.; Bader, R. F. W.; Tang, T.-H. *J. Comput. Chem.* **1982**, *3*, 317.

(22) Saunders, V. R.; Dovesi, R.; Roetti, C.; Causà, M.; Harrison, N. M.; Orlando, R.; Sicovich-Wilson, C. M. *CRYSTAL98 User's Manual*; University of Torino: Torino, 1998.

(23) Gatti, C. *TOPOND98 User's Manual*; CNR-CSRSRC: Milano, Italy, 1999.

(24) Koritsanszky, T.; Howard, S.; Mallison, P. R.; Su, Z.; Ritcher, T.; Hansen, N. K. XD. A computer Program Package for Multipole Refinement and Analysis of Electron Densities from Diffraction Data. *User's Manual*; Free University of Berlin: Germany, 1995.

(25) Pinkerton, A. A.; Schwarzenbach, D. ACA National Meeting, Hamilton, Ontario, Canada, June 22−27, 1986; Abstract PA22.

(26) Blessing, R. H. *Cryst. Rev.* **1987**, *1*, 3.

(27) DeTitta, G. T. *J. Appl. Crystallogr.* **1985**, *18*, 75.

(28) Sheldrick, G. M. *SHELXTL*, Vers. 5.1; An Integrated System for Solving, Refining and Displaying Crystal Structures from Diffraction Data. University of Göttingen: Germany, 1997.

(29) Allen, F. H.; Kennard, O.; Watson, D. G.; Brammer, L.; Orpen, A. G.; Taylor, R. *J. Chem. Soc., Perkin Trans. 2* **1987**, S1.

(30) Becker, P. J.; Coppens, P. *Acta Crystallogr.* **1974**, *A30*, 129.

(31) Hirshfeld, F. L. *Acta Crystallogr.* **1976**, *A32*, 239.

(32) Bader, R. F. W. *Atoms in Molecules: A Quantum Theory*; Clarendon Press: Oxford, 1990; Section 3.2.4.

(33) Abramov, Yu, A.; Volkov, A. V.; Coppens, P. *Chem. Phys. Lett.* **1999**, *311*, 81.

(34) (a) Spackman, M. A.; Byrom, P. G.; Alfredsson, M.; Hermansson, K. *Acta Crystallogr.* **1999**, *A55*, 30. (b) Silvestrelli, P. G.; Parrinello, M. *Phys. Rev. Lett.* **1999**, *82*, 3308.